Lattice Distortion Stabilizes the Photoinduced Metallic Phase in the Charge-Ordered Organic Salts (BEDT-TTF)$_3X_2$ ($X = ReO_4$, ClO_4)

Naoko Takubo,[1] Naoya Tajima,[1] Hiroshi M. Yamamoto,[1,2,3] HengBo Cui,[1] and Reizo Kato[1]

[1]*RIKEN, Hirosawa 2-1, Wako-shi, Saitama 351-0198, Japan*

[2]*JST-PRESTO, Honcho, Kawaguchi, Saitama 332-0012, Japan*

[3]*Institute for Molecular Science, Myodaiji, Okazaki, Aichi 444-8585, Japan*

(Received 17 July 2012; published 28 May 2013)

Photoinduced effects caused by intramolecular excitation were investigated by simultaneous optical and transport measurement in two charge-ordered organic salts, (BEDT-TTF)$_3X_2$ ($X = ReO_4$, ClO_4) [BEDT − TTF = bis(ethylenedithio)tetrathiafulvalene]. Although the two salts have the same molecular (average) charge and arrangement, they showed different photoinduced effects. A photoinduced insulator-to-metal phase transition with a metastable charge order-melting state was observed in the ReO_4 salt where the charge ordered state is associated with the lattice distortion. On the other hand, no photoinduced insulator-to-metal phase transition was noted in the ClO_4 salt where the charge ordered state is not accompanied by the lattice distortion. This comparative study suggested that the lattice distortion plays a key role in the stabilization of the photoinduced phase.

DOI: 10.1103/PhysRevLett.110.227401 PACS numbers: 78.55.Kz, 78.47.dc

Photoinduced phase transition (PIPT) has triggered much interest in both potential application to optoelectronics and basic condensed matter, especially in terms of photoinduced correlation among charge, spin, orbital, and structure. Internal multistability in the potential energy plays a key role in PIPT [1]. Accordingly, strong multiple interactions, such as electron-electron interaction and electron-lattice interaction are naturally expected in a PIPT system. Actually, a variety of PIPTs have been reported mainly in materials that undergo structural changes, namely those that show strong electron-lattice interaction [2–4]. A typical example of PIPT is the photoinduced insulator-to-metal transition (PIMT) that results from charge-order (CO) melting in a system where the CO state originates from the first-order transition with lattice distortion [5,6]. However, it has not yet been experimentally confirmed whether lattice distortion is essential in PIPT or not.

Among a variety of known CO materials, BEDT-TTF [BEDT-TTF = bis(ethylenedithio)tetrathiafulvalene] salts, which are low-dimensional organic conductors, exhibit various CO states depending on the counter anions, the spatial arrangements of BEDT-TTF molecules, and band filling. However, photoinduced CO melting in the BEDT-TTF salts has been studied in only two salts, α-(BEDT-TTF)$_2$I$_3$ (α-I$_3$) and θ-(BEDT-TTF)$_2$RbZn(SCN)$_4$ (θ-RbZn) [7,8]. Both of them show a horizontal-stripe CO pattern and a first-order CO insulator-to-metal transition with lattice distortion [9,10]. Comparative studies of the photoinduced CO melting associated with charge-transfer (CT) intermolecular excitation were performed by femtosecond pump and probe spectroscopy of both α-I$_3$ and θ-RbZn [8] and ultrafast local CO melting was observed in both. In θ-RbZn, the local CO melting immediately decayed. On the other hand, a long-lived quasistable CO-melting phase with a long decay time [$\sim$ nanosecond (ns) order] was observed in α-I$_3$. As for α-I$_3$, an anomalous photocurrent was observed when ns pulsed laser was irradiated at its CO state [7]. The photocurrent showed long-lived drastic conductivity enhancement, which indicates that the transition from the CO state to the conducting state is PIMT. A theoretical study also suggested that the photoinduced CO melting occurs more easily in α-I$_3$ than in θ-RbZn, because the lattice distortion, which is correlated to the stability of the CO state, is smaller in α-I$_3$ than in θ-RbZn [11].

It remains an open question whether the photoinduced CO-melting state is macroscopically stabilized by the lattice distortion in BEDT-TTF salts. In this study, therefore, we focused on (BEDT-TTF)$_3$(ClO$_4$)$_2$ (ClO_4 salt), which shows a second-order metal-to-CO insulator transition with no lattice distortion, in order to shed light on the above question. Moreover, we compared photoinduced phenomena in the ClO_4 salt with those in (BEDT-TTF)$_3$(ReO$_4$)$_2$ (ReO_4 salt). The latter has the same molecular arrangement and band filling as the ClO_4 salt and shows a first-order metal-to-CO insulator transition with lattice distortion. Specifically, we measured both optical and transport properties to investigate the photoinduced state induced by intramoleculer excitation.

(BEDT-TTF)$_3X_2$ ($X = ReO_4$, ClO_4) has two-dimensional conductive BEDT-TTF cation layers that are separated from each other by an anion layer. BEDT-TTF molecular arrangement in the conductive layer is the so-called β''-type, as shown in Figs. 1(a) and 1(b) [12,13]. (BEDT-TTF)$_3X_2$ ($X = ReO_4$, ClO_4) has a two-dimensional 1/3-filled hole band and shows a metal-to-insulator transition (MIT) with $T_C = 100$ K for the ReO_4 salt and 170 K for the ClO_4 salt [14,15]. The origin

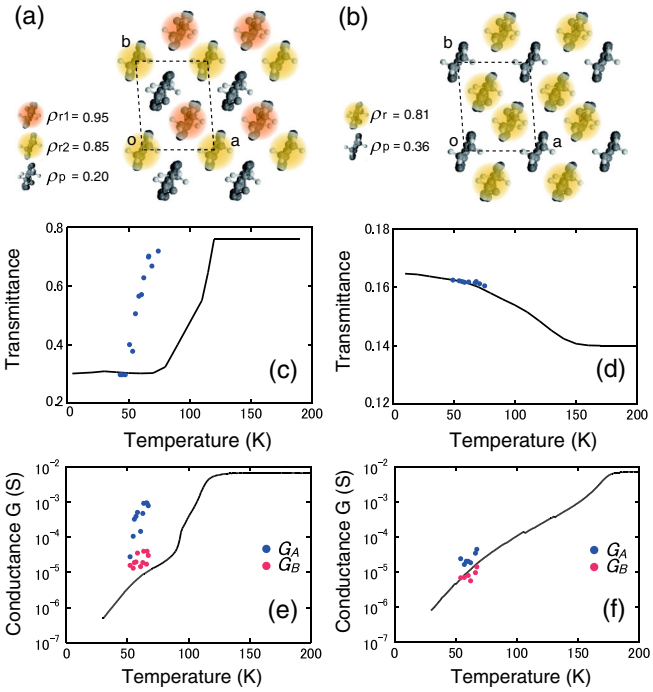

FIG. 1 (color online). Packing of BEDT-TTF molecules in (a) the ReO_4 salt and (b) the ClO_4 salt viewed from the long axis of BEDT-TTF molecules. Colored circles on the BEDT-TTF molecules represent charge-rich states at the CO insulator state. Temperature dependence of transmittance at 0.75 eV for (c) the ReO_4 salt and (d) the ClO_4 salt (solid line). Closed circles show correlations between T_{cal} and peak values of transmittance after light irradiation at 40 K for excitation light intensity $I_{exc} =$ 0–5 mJ/cm^2, where T_{cal} is the estimated temperature assuming that the absorbed light is completely converted into heat in the sample temperature dependence of electrical conductance G for (e) the ReO_4 salt and (f) the ClO_4 salt (solid line). Closed circles represent the calculated temperature T_{cal} of the fast coefficient G_A (blue circles) and slow coefficient G_B (red circles) of the conductance with excitation light irradiation at 40 K for excitation light intensity $I_{exc} = 1$–3 mJ/cm^2.

of MIT is charge ordering, as confirmed by far-IR and Raman spectroscopy [16,17]. In the ReO_4 salt, the site charge disproportionation ρ in the metallic state ($\rho_{r1,2} = 0.76$, $\rho_p = 0.48$) discontinuously changes at T_C ($\rho_{r1} = 0.95$, $\rho_{r2} = 0.85$, $\rho_p = 0.20$). The MIT shows not a superlattice but a remarkable discontinuous change in the molecular arrangement and the lattice constant with symmetric change ($P2_1/n$ at 300 K, $P2_1$ at 22 K) [16]. Provided that the extent of charge disproportionation is the order parameter, discontinuous change of ρ at T_C indicates that the MIT is a first order transition. On the other hand, in the ClO_4 salt, the ρ value is almost constant in the metallic state ($\rho_{r1,2} = 0.75$, $\rho_p = 0.50$) and continuously splits below T_C down to 10 K ($\rho_{r1,2} = 0.81$, $\rho_p = 0.36$) [17]. Therefore, the MIT in the ClO_4 salt is a second order transition. It was also confirmed by specific heat measurement that the MIT is a second-order transition [15]. The MIT shows no distinguishable change in molecular arrangement with no symmetric change ($P\bar{1}$) [18]. Therefore, the charge localization in the ClO_4 salt is attributed to a purely electronic origin. The MIT for each salt was also studied by mid-IR spectroscopy [19,20]. Reflectivity along [012] at 0.8 eV, which is in the CT band, discontinuously changes at T_C with hysteresis in the ReO_4 salt, whereas it exhibits a continuous change below T_C without hysteresis in the ClO_4 salt.

We simultaneously measured both conductance and transmittance in a plane parallel to the conductive layer of a sample that was irradiated with a pulsed laser. $(BEDT\text{-}TTF)_3X_2$ thin crystals were prepared by an electrochemical method. The thin crystal samples had flat surfaces, which were parallel to conductive layers. A typical sample measured 0.8×0.5 mm^2 in area and 500 nm in thickness. A sample was excited with a pulsed laser generated by an optical parametric oscillator with the third harmonic of a pulsed YAG laser. The pulsed laser had a pulse width of 5 ns, an excitation energy of 2.76 eV, and a spot diameter of 2.5 mm. The polarization of the laser light was parallel to a conductive layer. The excitation energy is comparable to a HOMO-LUMO gap of a BEDT-TTF neutral molecule, which is about 2.5 eV (intramolecular excitation). It should be noted that the light penetration depth at 2.76 eV is approximately 1 μm [7], which is sufficiently larger than the sample thickness and therefore, enables excitation of the entire sample area. Accordingly, transmittance and conductance change can be evaluated in terms of bulk properties. The transmittance at 0.75 eV, which is in the CT band [19,20], was probed with a continuous-wave diode laser. Figures 1(c) and 1(d) present the temperature dependence of the transmittance at 0.75 eV in (c) the ReO_4 salt and (d) the ClO_4 salt (solid line). As shown in Fig. 1(c), the transmittance in the ReO_4 salt exhibits a discontinuous change around T_C, which is caused by the first-order MIT. On the other hand, the transmittance in the ClO_4 salt features a continuous change below T_C, as shown in Fig. 1(d). In both cases, the transmittance at 0.75 eV can be used as a probe of PIMT. The voltage change of a pulsed laser irradiated sample was measured with an oscilloscope connected to the sample in series [as shown in the inset of Fig. 2(d)]. Two carbon paste electrodes were formed on a sample surface (conductive plane). Both the length and distance of the electrodes were on the orders of 100 μm. Conductance G of the sample was estimated by $G = (V/R)/(V_0 - V)$, where V_0 is the applied voltage to the sample, R is the reference resistance of the oscilloscope (50 Ω), and V is the measurement voltage of the oscilloscope. The voltage V_0, which has a pulse width of 75 μs, was applied to a sample 10 μs before the excitation pulse irradiation. The time resolution was 5 ns. We checked the linear I-V characteristics in the absence of laser irradiation, the negligible heating effect due to probe light absorption, and the

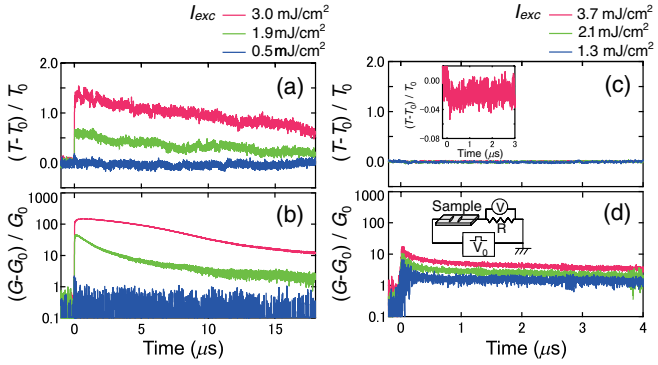

FIG. 2 (color online). Time evolution of (a) transmittance and (b) conductance in the ReO_4 salt and (c) transmittance and (d) conductance in the ClO_4 salt at 40 K for various excitation light intensities I_{exc}. The inset of Fig. 2(c) shows magnified transmittance change for $I_{exc} = 3.7$ mJ/cm^2. The inset of Fig. 2(d) shows the circuit for conductance measurement. The photon energy of the excitation pulse was 2.76 eV. The probe light energy was 0.75 eV. The applied electric field was 80 V/cm for the ReO_4 salt and 400 V/cm for the ClO_4 salt.

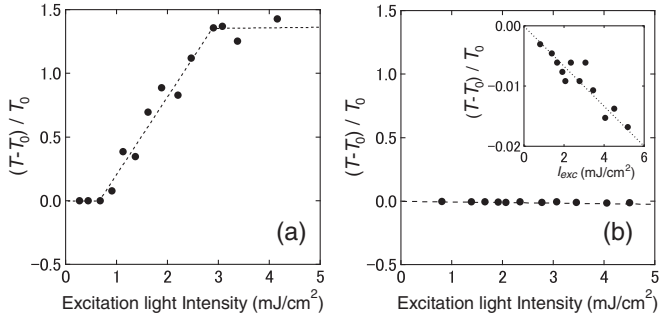

FIG. 3. Relationship between excitation light intensity I_{exc} and peak values of transmittance for (a) the ReO_4 salt and (b) the ClO_4 salt at 40 K. The photon energy of the excitation pulse was 2.76 eV. The inset of Fig. 3(b) shows magnified transmittance change. The probe light energy was 0.75 eV. Dotted lines are guides for the eyes.

negligible heating effect due to applied voltage in this measurement. It was experimentally confirmed that neither the light polarization direction nor electric field direction in the conductive layer was significant in this study.

Figure 2 shows the time evolution of transmittance (a) and conductance (b) after the pulsed laser irradiation (with intensity I_{exc}) of the ReO_4 salt in the CO state at 40 K. Although the transmittance did not change for $I_{exc} = 0.5$ mJ/cm^2, it increased within 5 ns immediately after the laser irradiation for $I_{exc} = 1.9$ and 3.0 mJ/cm^2. Both transmittance peak and lifetime increased as I_{exc} increased. The peak value of the transmittance for $I_{exc} = 3.0$ mJ/cm^2 in Fig. 2(a) is 0.70, which is comparable to that in the high-temperature metallic phase [0.76, Fig. 1(c)]. The conductance in Fig. 2(b) also increased after the laser irradiation with $I_{exc} = 1.9$ and 3.0 mJ/cm^2. Moreover, both the conductance peak and lifetime obviously increased as I_{exc} increased. In the case of $I_{exc} = 3.0$ mJ/cm^2, the conductance increased by 3 orders of magnitude and reached a value that was comparable to that in the high-temperature metallic phase. These results suggest that the light irradiation induces a macroscopic metallic state associated with the CO melting.

On the other hand, in the ClO_4 salt, when the pulsed laser was irradiated at 40 K, the transmittance remained nearly constant, as shown in Fig. 2(c). By contrast, the conductance demonstrated a significant change, as can be seen in Fig. 2(d). The conductance peak increased as I_{exc} increased and the peak value of 5×10^{-5} S for $I_{exc} = 3.7$ mJ/cm^2 is approximately one-hundredth of the value in the high-temperature metallic phase.

Figure 3 presents the relationship between excitation light intensity I_{exc} and peak values of transmittance at 40 K. In the ReO_4 salt [Fig. 3(a)], the transmittance remains unchanged until the excitation light intensity reaches the threshold, $I_{th} \sim 1$ (mJ/cm^2). The I_{exc} value of 1 mJ/cm^2 is comparable to 1 photon per 110 BEDT-TTF molecules. Above the threshold value, the transmittance increases monotonically and saturates above $I_{sat} \sim 3$ mJ/cm^2. In contrast, the ClO_4 salt shows little change of the transmittance [Fig. 3(b)]. The transmittance peak value continuously decreases as I_{exc} increases without any threshold, as observed in the inset of Fig. 3(b).

According to a previous study of α-I_3, both I_{th} and I_{sat} are associated with a metastable photoinduced phase [21]. The threshold observed in the ReO_4 salt indicates that the photo-induced metallic state should originate in cooperative effects. The saturation of the transmittance indicates that the entire area of the sample becomes metallic. Accordingly, the photoinduced CO-melting phase is macroscopically stabilized, namely, PIMT occurs in the ReO_4 salt.

Then, we evaluated the heating effects of the laser irradiation on the sample. The temperature increase of the sample, ΔT in K, is calculated assuming that the absorbed light is completely converted into heat in the sample. The temperature dependence of heat capacity C_P, in J K^{-1} mol^{-1}, of the sample is experimentally obtained as $C_P = 5T$, where T is the temperature in K [22]. The laser pulse intensity I_{exc} can be approximated by a Gaussian function with 5 ns in width. The temperature of the sample after the laser irradiation T_{cal}, in K, is given by $T_{cal} = \Delta T + 40$, when the laser irradiation is carried out at 40 K.

The peak values of the transmittance after the light irradiation at T_{cal} for $I_{exc} = 0$–5 mJ/cm^2 are plotted in Fig. 1(c) for the ReO_4 salt and in Fig. 1(d) for the ClO_4 salt. As for the ReO_4 salt, the peak values of the transmittance after the light irradiation are much larger than the transmittance at T_{cal} with no irradiation, which indicates that the drastic transmittance change cannot be explained by the temperature increase due to the light absorption. On the other hand, in the ClO_4 salt, the values well follow the

temperature dependence of the transmittance with no irradiation and thus, the behavior of the transmittance in the ClO_4 salt can be explained by the temperature effect due to the light absorption.

Next, we discuss the conductance change after the light irradiation. A two- (first and slow) component exponential curve $G_A \exp(-t/\tau_1) + G_B \exp(-t/\tau_2)$ is used to analyze the time profiles in Figs. 2(b) and 2(d). This works well, as shown in the insets in Fig. 4. First, we examine the heating effect due to the light absorption. Coefficients G_A and G_B at T_{cal} for $I_{exc} = 1$–3 mJ/cm^2 are plotted in Fig. 1(e) for the ReO_4 salt and in Fig. 1(f) for the ClO_4 salt. Coefficient G_B of the slow decay component of the ClO_4 salt is comparable to the conductance under the no irradiation condition at T_{cal}; thus, the slow decay component should be explained by the temperature increase due to the light absorption. On the other hand, coefficient G_A of the fast decay component is larger than the conductance under the no irradiation condition. Unlike the transmittance change, therefore, the conductance change after the light irradiation has another component that cannot be explained by the heating due to the light absorption. As for the ReO_4 salt, coefficient G_A should originate from PIMT. Although coefficient G_B slightly deviates from the conductance under the no irradiation condition, it would be associated mainly with the temperature effect due to the light absorption. It seems that the conductance relaxation for PIMT is nonlinear and cannot be explained by a simple exponential decay. Note that the decay time τ_2 is 10^{-5} (s) order in both salts. Second, we examine the fast decay component by focusing on decay time τ_1. Figures 4(a) and 4(b) show the correlation between excitation light intensity I_{exc} and decay time τ_1 for both salts at 40 K. As for the ReO_4 salt, τ_1 increases with increasing I_{exc}. This indicates that the lifetime of the CO-melting domains increases as the domain size increases, namely, there exist multiple interactions in the metastable CO-melting domains. On the other hand, τ_1 in the ClO_4 salt is constant and independent of I_{exc}, which suggests that the fast decay component in the ClO_4 salt does not originate from PIMT. It may be attributed to the photoconductivity that is not related to the CO melting.

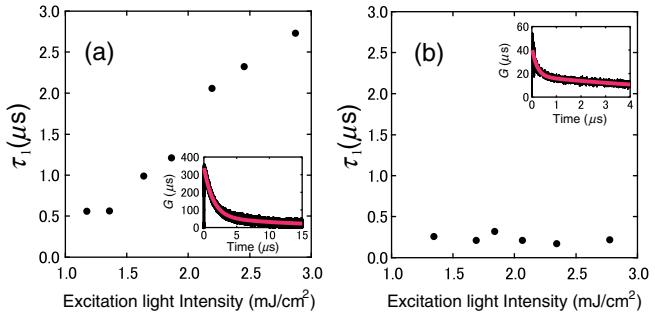

FIG. 4 (color online). Relationship between excitation light intensity I_{exc} and fast decay time τ_1 of conductance in (a) the ReO_4 salt and (b) the ClO_4 salt at 40 K. The inset shows the time profile of conductance with light irradiation I_{exc} = (a) 1.9 and (b) 2.1 mJ/cm^2 (black line) and two-component exponential curve fitting (red line). The photon energy of the excitation pulse was 2.76 eV. The applied electric field was 80 V/cm for the ReO_4 salt and 400 V/cm for the ClO_4 salt.

In view of the above experimental results, the photoinduced CO-melting metallic phase, or PIMT, was observed only in the ReO_4 salt where the original CO formation is a first-order transition accompanied by lattice distortion. On the other hand, in the ClO_4 salt where the CO formation is a second-order transition, both transmittance and conductance did not show any of the changes that were expected for PIMT. In addition, it is important to note that we performed same experiments up to 130 K in the ClO_4 salt and obtained the same results. We now discuss the stability of the CO-melting state. When a sample in the CO state is irradiated with excitation light, local photocarriers disturb the CO state and consequently the local CO-melting state is formed. In this regard both electron-electron interaction and electron-molecular-vibration coupling should play a key role in forming the CO-melting state [23]. In the ReO_4 salt, lattice distortion is restored by electron-lattice interaction in the CO-melting state because free energy of the metallic state decreases due to the restored lattice distortion. Such a CO-melting state accompanied by structural changes would be retained as long-lived CO-melting domains after deexcitation. Furthermore, many CO-melting domains should condense and form a stabilized photoinduced phase. On the other hand, a local CO-melting state should not be accompanied by structural changes in the ClO_4 salt, and immediately decay to the original CO state after deexcitation. As a result, the local CO-melting state cannot be stabilized as macroscopic (meta)stable domains. Therefore, PIMT does not occur in the ClO_4 salt. These experimental results strongly support the idea that PIMT is the phase transition to a (meta)stable phase stabilized by lattice distortion.

It should be added that the photoinduced CO melting that involves a larger lattice distortion is more difficult to occur as described in the Introduction [8,11]. For example, in the case of θ-RbZn that has a large lattice distortion forming large molecular rotation and a superlattice in the CO formation [10], a large lattice distortion requires a long time for restoration compared to the relaxation time of the local photoinduced CO-melting state. Consequently, the photoinduced CO-melting state in this case cannot be stabilized as macroscopic (meta)stable domains. Therefore, electron-lattice interaction plays an important role in PIMT in CO-BEDT-TTF salts. Specifically, moderate electron-lattice interaction should stabilize macroscopic (meta)stable CO-melting domains.

In conclusion, the photoinduced effect in the CO state was investigated in two BEDT-TTF systems (ReO_4 and ClO_4 salts). Both optical transmittance and electrical conductance changes clearly showed that PIMT occurs

only in the ReO_4 salt where CO formation involves lattice distortion. On the other hand, in the ClO_4 salt where CO formation is purely electronic, the photoinduced behavior can be explained by the heating effect and photoconductivity that does not originate from PIMT, namely, the ClO_4 salt does not show PIMT. All experimental results indicate that lattice distortion is essential for the stability of the photoinduced CO-melting phase in the CO-BEDT-TTF salts.

The authors thank Dr. Kenji Yonemitsu and Dr. Takashi Oka for fruitful discussions. This research was partially supported by Grant-in-Aid for Scientific Research (S) (No. 22224006) from the Japan Society for the Promotion of Science (JSPS).

[1] *Photoinduced Phase Transition*, edited by K. Nasu (World Scientific, Singapore, 2004); Y. Tokura, J. Phys. Soc. Jpn. **75**, 011001 (2006).
[2] S. Koshihara, Y. Tokura, T. Mitani, G. Saito, and T. Koda, Phys. Rev. B **42**, 6853 (1990).
[3] A. Cavalleri, Cs. Toth, C. W. Siders, J. A. Squier, F. Raksi, P. Forget, and J. C. Kieffer, Phys. Rev. Lett. **87**, 237401 (2001).
[4] S. Ohkoshi, H. Tokoro, and K. Hashimoto, Coord. Chem. Rev. **249**, 1830 (2005).
[5] K. Miyano, T. Tanaka, Y. Tomioka, and Y. Tokura, Phys. Rev. Lett. **78**, 4257 (1997).
[6] M. Chollet, L. Guerin, N. Uchida, S. Fukaya, H. Shimoda, T. Ishikawa, K. Matusda, T. Hasegawa, A. Ota, H. Yamochi, G. Saito, R. Tazaki, S. Adachi, and S. Koshihara, Science **307**, 86 (2005).
[7] N. Tajima, J. Fujisawa, N. Naka, T. Ishihara, R. Kato, Y. Nishio, and K. Kajita, J. Phys. Soc. Jpn. **74**, 511 (2005).
[8] S. Iwai, K. Yamamoto, A. Kashiwazaki, F. Hiramatsu, H. Nakaya, Y. Kawakami, K. Yakushi, H. Okamoto, H. Mori, and Y. Nishio, Phys. Rev. Lett. **98**, 097402 (2007).
[9] T. Kakiuchi, Y. Wakabayashi, H. Sawa, T. Takahashi, and T. Nakamura, J. Phys. Soc. Jpn. **76**, 113702 (2007).
[10] M. Watanabe, Y. Noda, Y. Nogami, and H. Mori, J. Phys. Soc. Jpn. **73**, 116 (2004).
[11] Y. Tanaka and K. Yonemitsu, J. Phys. Soc. Jpn. **79**, 024712 (2010).
[12] H. Kanbara, H. Tajima, S. Aratani, K. Yakushi, H. Kuroda, G. Saito, A. Kawamoto, and J. Tanaka, Chem. Lett. **1986**, 437 (1986).
[13] H. Kobayashi, R. Kato, T. Mori, A. Kobayashi, Y. Sasaki, G. Saito, T. Enoki, and H. Inokuchi, Chem. Lett. **1984**, 179 (1984).
[14] S. S. P. Parkin, E. M. Engler, V. Y. Lee, and R. R. Schumaker, Mol. Cryst. Liq. Cryst. **119**, 375 (1985).
[15] T. Enoki, K. Tsujikawa, K. Suzuki, A. Uchida, Y. Ohashi, H. Yamakado, K. Yakushi, and G. Saito, Phys. Rev. B **50**, 16 287 (1994).
[16] T. Yamamoto, M. Uruichi, K. Yakushi, J. I. Yamaura, and H. Tajima, Phys. Rev. B **70**, 125102 (2004).
[17] T. Yamamoto, M. Uruichi, K. Yakushi, and A. Kawamoto, Phys. Rev. B **73**, 125116 (2006).
[18] See Supplemental Material at http://link.aps.org/supplemental/10.1103/PhysRevLett.110.227401 for crystal structure of $(BEDT\text{-}TTF)_3(ClO_4)_2$ single crystal.
[19] K. Yakushi, H. Kanbara, H. Tajima, H. Kuroda, G. Saito, and T. Mori, Bull. Chem. Soc. Jpn. **60**, 4251 (1987).
[20] H. Tajima, H. Kanbara, K. Yakushi, H. Kuroda, G. Saito, and T. Mori, Synth. Met. **25**, 323 (1988).
[21] N. Takubo, N. Tajima, H. M. Yamamoto, and R. Kato, J. Lumin. **137**, 237 (2013).
[22] S. Yamashita (private communication).
[23] Y. Kawakami, T. Fukatsu, Y. Sakurai, H. Unno, H. Itoh, S. Iwai, T. Sasaki, K. Yamamoto, K. Yakushi, and K. Yonemitsu, Phys. Rev. Lett. **105**, 246402 (2010).